Manipulating emission of CdSe/ZnS nanocrystals embedded in 3D photonic crystals

Céline Vion, Carlos Barthou, Paul Bénalloul, Catherine Schwob, Laurent Coolen, Alex Gruzintev, Gennadi Emelchenko, Wladimir Masalov, Jean-Marc Frigerio, Agnès Maître

Manipulating emission of CdTeSe nanocrystals embedded in 3D photonic crystals

Céline Vion[1],* Carlos Barthou[1], Paul Bénalloul[1], Catherine Schwob[1], Laurent Coolen[1], Alex Gruzintev[2], Gennadii Emel'chenko[3], Vladimir Masalov[3], Jean-Marc Frigerio[1], and Agnès Maître[1]

(1) Institut des NanoSciences de Paris, UMR-CNRS 7588, Université Pierre et Marie Curie, F-75015 Paris, France

(2) Institut of Microelectronics Technology and High Purity Materials, Russian Academy of Science, 142432, Chernogolovka, Moscow District, Russia and

(3) Institute of Solid State Physics, Russian Academy of Science, 142432, Chernogolovka, Moscow District, Russia

(Dated: February 14, 2009)

Abstract

We report experimental and theoretical results on the photoluminescence of CdTeSe nanocrystals, embedded in a silica opaline structure by infiltration of a highly diluted solution. Strong modification of emission diagrams of embedded nanocrystals have been observed in good agreement with theoretical models. At macroscopic scale, we measured the difference of lifetime between an opal infiltrated with nanocrystals with emission wavelength in the pseudogap and an opal with smaller balls size for which the nanocrystal emission wavelength is outside the pseudogap. The photonic bandgap effect leads a lifetime increase of the order of 10%. These lifetime variations are shown to be in good agreement with the calculated local density of states modification due to the pseudogap.

PACS numbers: 42.50.Nn; 42.70.Qs, 61.72.uj; 61.46.Hk; 78.67.Bf

*Electronic address: celine.vion@insp.jussieu.fr

I. INTRODUCTION

Photonic crystals are characterized by a periodic dielectric constant at wavelength scale, creating photonic energy bands where light propagation is forbidden. The emission of light sources embedded inside a photonic crystal can be strongly affected by these bandgaps: according to Fermi's golden rule, the spontaneous emission rate is proportional to the photonic local density of states (LDOS), which describes the interaction between emitters and the local field in the sample. As the photonic local density of states is strongly dependant on the material structure, photonic crystals are used for tailoring the emission of embedded light sources. This active field of research leads to applications ranging from quantum information processing [1], to light emitting devices (miniature lasers) [2] or solar cells [3].

Most devices use 2-dimensions (2D) photonic crystals, consisting in a lattice of holes etched in a high index transparent material. In the weak coupling regime, emission of single quantum dots in 2D photonic crystals has been improved, as well for their photoluminescence intensity [4] as for the polarization of emission [5]. In the strong coupling regime [6], achieved with InAs quantum dots embedded in a GaAs photonic crystal membrane, vacuum Rabi splitting [7] and emission of indistinguishable single photons [1] have been demonstrated. All these devices have been realized by electron lithography, requiring heavy technological equipments. Alternatively to this top-down approach, impregnation of 2D photonic crystals with solutions of colloïdal nanocrystals is a versatile way to couple emitters to photonic structures and to allow enhancement of spontaneous emission [8, 9].

3-dimensions (3D) photonic crystals take advantage of the spontaneous self organization of spherical colloidal particles. Indeed, various techniques provide a low-cost and relatively easy protocol to obtain synthetic opals. It has been shown that the quality of opaline structures strongly depends on synthesis techniques [10]. Just as in 2D photonic crystals, the spontaneous emission of optical sources embedded in direct and inverted opals is affected by the crystal structure and can be inferred by the local density of states [11]. However, the modification of spontaneous emission lifetime by 3D silica opals is reported to be weak since the refractive index contrast is low [12]. Larger effects require a higher refractive contrast and a complete photonic band gap which can be obtained in inverted opals [13–15]. For colloidal CdSe nanocrystals infiltrated in titania inverse opals, lifetime

reductions up to 30% have been reported [16]. Nevertheless, good quality inverse opals over large scale are still difficult to synthesize and most experimental studies on coupling emitters to 3D photonic crystals have been achieved in opals exhibiting a pseudo-band gap (infiltrated with nanocrystals [17–22] or molecules [14, 23–25]).
Even incomplete, the photonic bandgap affects both the luminescence spectrum of the emitter and its spontaneous lifetime. Nevertheless, disorder in opal structures can hide or limit these phenomena. To get rid of the disorder, experiments have to be performed at a scale smaller than the typical size of the opal for which it can be considered as a monocrystal. The use of a microscope can reveal the quality of the opals at a micronic scale by selection of a high quality opal zone [17, 25]. At this scale, stop-band effect on nanocrystals luminescence spectra [26], single nanocrystal emission modification [17] and sligth effects on luminescence lifetime [25] have been reported. Nevertheless the pseudo gap effect is averaged over the whole numerical aperture of the microscope objective, and the dip in fluorescence spectrum due to the gap disappears for a large aperture [23]. Therefore, the use of a microscope limits the possibilities to study angle-resolved luminescent properties and does not reveal the quality of the opal over a large scale (mm) which is essential for applications.

The aim of this work is to study at macroscopic scale the coupling of colloidal CdTeSe nanocrystals to artificial direct opals. In the first part, we present the preparation and optical characterization of opaline structures. The second section presents the modification of nanocrystals emission diagrams. In a third section, a lifetime modification due the photonic bandgap is evidenced and interpreted by LDOS calculations.

II. OPALS CHARACTERIZATION

Two opals, which will be called respectively A and B, were prepared by sedimentation of 400 nm and 270 nm diameter silica balls in suspension in water, with a post selection of the 0.5 mm thick upper part of the deposit. The balls got organized spontaneously as a face-centered-cubic (fcc) structure, the highest density plane (111) being along the slab plane. The samples were then dried at 150°C, and annealed at 600°C during 5 hours in free atmosphere. Robust 5x5x0.5 mm^3 samples were obtained ($\approx$ 2000 layers) [27, 28].

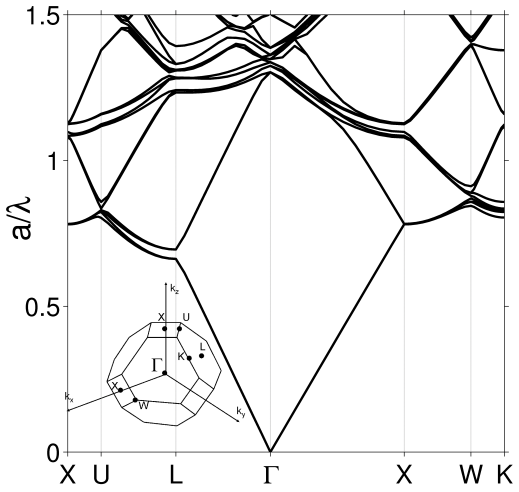

FIG. 1: Photonic band structure of the fcc lattice calculated with effective index n_{eff}=1.29 as a function of reduced frequency a/λ (where a is the primitive cell parameter $a = \sqrt{2}D$, with D the diameter of the balls), for wave vectors between the high symmetry points X, U, L, Γ, K and W of the Brillouin zone.

Figure 1 presents the opal band diagram calculated numerically by a direct computation of the eigenstates and eigenvalues of Maxwell's equations (using a planewave basis) [29], showing a photonic pseudogap at the L point of the photonic Brillouin zone.

The two opals were optically characterized by specular reflection, from which the diameter of the balls and the effective refracting index of the medium were inferred. The samples were illuminated with a fibered and collimated halogen source covering the whole 350-820nm spectral range, and the reflected light was collected by a second optical fiber symmetric to the first one. The fibers were mounted on rotating stages allowing a precise selection of the incident and collection angles. The light spot on the opal had a size of 4 mm^2(at 20° incidence) and the distances between the sample and the optical fibers were 10 cm.

As the first bandgap of the direct opal is not complete, light propagation in this frequency range is allowed for certain directions and prohibited for others. An important reflectivity is awaited for the wavelengths for which the phase difference induced by reflections on two consecutive (111) planes of the face-centered cubic lattice is a multiple of 2π. This condition is fulfilled for an incidence angle corresponding to the Bragg angle which can be expressed

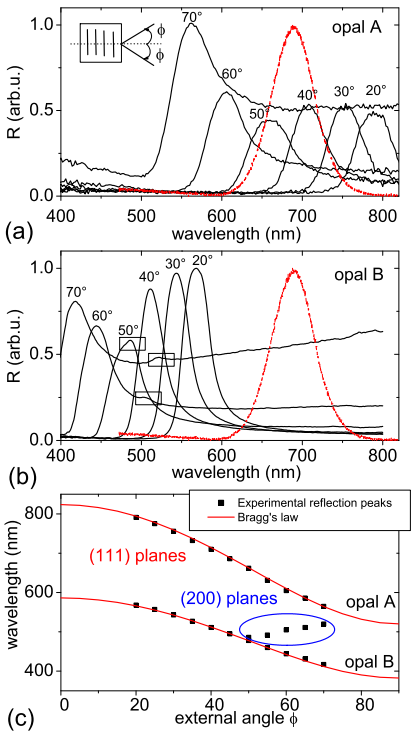

FIG. 2: Reflectivity spectrum of opals (a) A and (b) B for various incidence angles. (on figure (b) squares indicate the position of the second peaks). Red line: CdTeSe nanocrystals luminescence spectrum in decane, (c) Comparison of the experimental results with Bragg's law (Eq.1). opal A: $D_A = 391nm$, n_A^{eff}=1.29, opal B: $D_B = 269nm$ $n_B^{eff} = 1.34$

as [30]:

$$\lambda_{max} = 2\sqrt{(2/3)}D\sqrt{(n_{eff}^2 - \sin^2(\phi))} \quad (1)$$

where D is the diameter of the balls, ϕ is the incidence angle relative to the normal of the (111) plane and n_{eff} is the effective refractive index of the medium with $n_{eff} = \sqrt{\alpha\epsilon_{silica} + (1-\alpha)\epsilon_0}$, and α is the filling factor ($\alpha = 0.74$ for close packed structures).

Figures 2 (a) and (b) present the spectra obtained by specular reflection on the two opals for non polarized light at different incidence angles. The wavelengths for which the specular reflectivity is maximum are plotted according to the angle of incidence for the two opals. An adjustment with Bragg's law (fig. 2c) yields with a precision of 5% for the two samples the balls diameters $D_A = 391$ nm and $D_B = 269$ nm and the effective indices $n_A^{eff} = 1.29$ and $n_B^{eff} = 1.34$. The diameters are in good agreement with the measurements performed

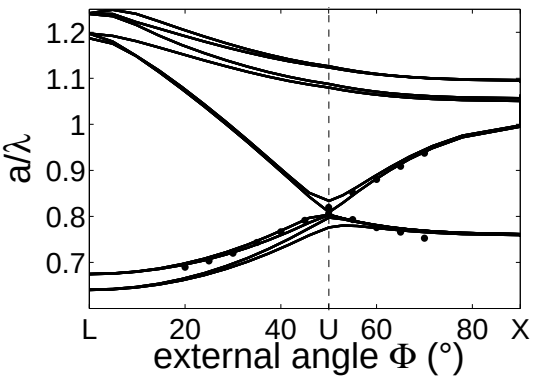

FIG. 3: Photonic band structure (solid line) calculated along the LU and UX line expressed as a function of incidence angle for 269nm balls size opal. The circles indicate the experimental peaks associated with (111) and (200) planes.

with an atomic force microscope. The measured effective indices correspond to a silica index $n_B^{silica} = 1.44$ for the smaller balls, and $n_A^{silica} = 1.39$ for the larger balls. The difference between these two values may be attributed to a more porous silica structure in larger balls [31].

At an angle ϕ larger than 50°, a second peak can be distinguished on the reflection spectra on figure 2(b). This peak unlike the first one shifts toward higher wavelengths for increased incident angles, as described in PMMA-sphere opals [32]. The interpretation of this phenomenon requires exact band structure calculations. On figure 3 the photonic band structure calculated along the LU and UX lines inside the first Brillouin zone (for $n_B^{eff} = 1.34$) is superimposed on the experimental peaks of specular reflection spectra as a function of the external incidence angle ϕ, which is related by Snell's law $\sin(\phi) = n_B^{eff} \sin(\theta)$ to the internal angle θ with the L direction normal to the (111) plane. At the U point (corresponding to an external angle ϕ of 50.2°), a second pseudo-gap can be attributed to the constructive interference reflections on the planes (200).

III. MODIFICATION OF NANOCRYSTALS EMISSION SPECTRA

We focus first on emission spectra modifications of nanocrystals embedded in the opal. We use a nanomolar solution of CdTeSe nanocrystals [33] diluted in decane of index $n_{decane} = 1.41$, a value close to the measured silica index for large balls size($n_B^{silica} = 1.39$). The

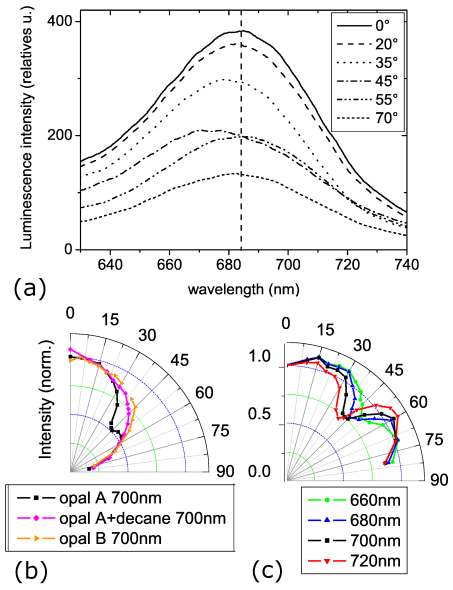

FIG. 4: (a) Luminescence spectra of infiltrated nanocrystals in opal A sample at different collection angles. (b) Diagrams of radiation in polar representation at 700 nm of CdTeSe nanocrystals in opal A (black line) compared to nanocrystals in opal A infiltrated with decane (purple line) and in opal B (orange). (c) Diagrams of radiation of infiltrated CdSeTe nanocrystals in opal A at different wavelengths normalized with respect to the corresponding reference diagrams in the decane infiltrated opal.

luminescence spectrum of the solution is centered at 685 nm and presents a Full Width Half Maximum (FWHM) of 60 nm (see fig. 2). These nanocrystals exibit a good photostability. Their decay time (45ns in decane) is longer than for standard CdSe nanocrystals.
Both opals are infiltrated with $1\mu L$ of this solution and become translucent, demonstrating that the solution spread all over the opal: the decane infiltrated opal is equivalent to an homogeneous medium with an effective index of 1.39. As a consequence, the nanocrystals are distributed randomly in the whole volume of the sample, with much less than one nanocrystal per void. Indeed, this low density of emitters prevents nanocrystals aggregation and interactions among them, and the optical properties of the opal are not modified : after 15 min, the decane solution is totally evaporated, and specular reflection spectra realized on the infiltrated opal are identical to the ones realized prior to infiltration.

The infiltrated nanocrystals are then excited at a wavelength of 337.1 nm by a pulsed nitrogen laser (0.6 ns pulse width). Their luminescence is collected by an optical fiber

mounted on a rotary stage and located at a distance of 10 cm from the surface. In this setup, for an illumination spot of $1mm^2$ size on the opal surface, the detection angle resolution is approximately 1°. The emission is analyzed with a spectrometer coupled to a nitrogen-cooled Si Charged-Coupled Device (CCD) detector. This setup has a wavelength resolution of 0.3 nm/point. The experimental specular spectra of opal A infiltrated with nanocrystals are plotted in figure 4(a) for different collection angles. As the FWHM of quantum dots luminescence spectrum is of the same order as the stop band FWMH, the incidence angle dependent gap does not induce a dip on luminescence spectra but induces a shift of the peak wavelength (see fig. 4(a)). Depending of the angle of collection, the central wavelength of the emission line is shifted from 685nm to 670nm for incidence angles from 0° to 45°. In figure 4(b), the radiation diagrams at 700nm is plotted as a function of the angle of detection ϕ. A reduction of luminescence is observed at 45°. In order to confirm the influence of the crystalline structure, the infiltrated opal A is filled with a solution of decane, removing the gap. The dip in the emission diagram of nanocrystals disappears for the decane filled sample, as expected for an homogeneous medium (fig. 4(b)).

On figure 4(b), we also plot the emission diagram at 700nm for opal B. No dip appears and the emission diagram is similar to the diagram of the opal A filled with decane. For this opal, the gap at 0° incidence is at 589nm (see fig. 2(b)) so that emission at 700nm is well above the bandgap. In this part of the band structure the sample is equivalent to an homogeneous medium (see fig. 1 for $a/\lambda = 0.54 < 0.62$), so that this opal, like the decane infiltrated opal, can serve as a reference for which no bandgap effect is expected.

In figure 4(c), we plot for different wavelengths the radiation diagrams normalized with respect to the corresponding reference diagrams in the decane infiltrated opal. For each wavelength, the luminescence reduction is observed for specific angles. In figure 5, these specific wavelengths for which quantum dots luminescence is reduced, are plotted as a function of the external angle ϕ. The curve is fitted by Bragg's law, like the central wavelength photonic bandgap measured previously by specular reflection (fig. 2). These results are a clear demonstration of the modification of nanocrystals spontaneous emission diagrams by the photonic bandgap.

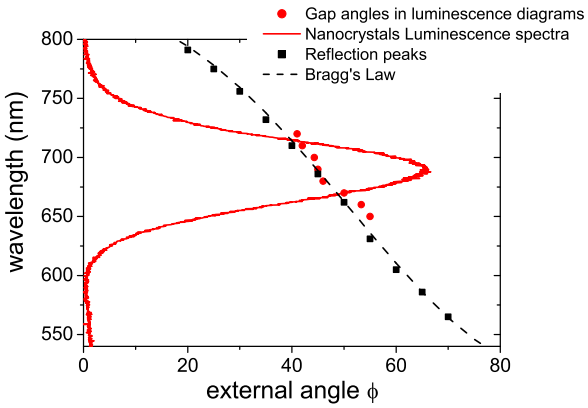

FIG. 5: Comparison of the experimental results with Bragg's law for opal A. Red line: nanocrystals in decane luminescence spectra. The red circles indicate the position of the minima on the diagrams of radiation. The black squares are the positions of the reflection maxima. The dotted line is a fit of the reflexion maxima by Bragg's law with parameters $D_A = 391nm$ and $n_A^{eff} = 1.29$.

IV. MODIFICATION OF NANOCRYSTALS EMISSION LIFETIME

Let us now consider the influence of the photonic crystal on the nanocrystals emission decay rate. We experimentally compare the lifetime of nanocrystals embedded in opals A ($D_A = 391nm$) and B ($D_B = 269nm$). Their gaps are respectively located at 824nm and 589nm at 0° incidence. We performed the experiments at 700nm by selecting spectrally through a monochromator the emission of the nanocrystals. For this wavelength, the nanocrystal emission is located inside the gap for opal A and outside the gap for opal B. The samples are kept in vacuum to prevent nanocrystal oxydation, since we observed a lifetime decrease of a few nanoseconds over tens of minutes when the experiment was performed in air. The decay curves are measured by a photomultiplier coupled to an oscilloscope. The time constant of the setup is of one nanosecond. In the following, the fiber is normal to the surface. Each measurement was performed at six different locations on both opals.

The decay analysis has to be very careful because the expected lifetime modification is rather weak for low index contrast opals as reported in the literature [12, 25]. As seen on figure 6, opals exhibit self-luminescence under 337nm excitation wavelength, but this luminescence decay is much faster than the nanocrystals one. It can be seen on the emission

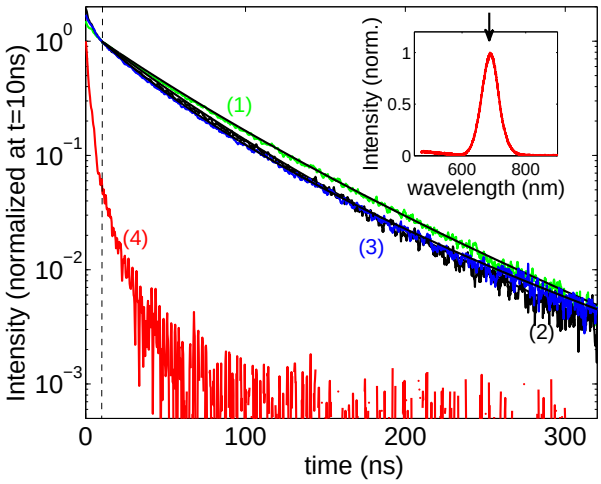

FIG. 6: Decays measured at 700nm for 381nm balls size opal. (1) Luminescence decay of nanocrystals infiltrated in the opal A (green line), (2) nanocrystals in opal B (black line), (3) nanocrystals in the opal A infiltrated with decane (blue line). (4) Red line: self-luminescence of the opal. The fits using the log-normal distribution are plotted in black. The inset presents the luminescence spectrum in opal A at 0° collection.

spectrum (inset on fig. 6) that, for such pulsed excitation, the self luminescence is more than 10 times less intense than the nanocrystals emission. If, for times shorter than 10 ns, the fast self-luminescence of silica balls influences the decay curves, after 10 ns it can be considered as negligible. The nanocrystal luminescence lifetimes are therefore calculated by fitting the decay curves for times between 10ns and 320ns. We fit the non-exponential decay curves with a continuous log-normal distribution of decay rates as suggested in reference [34] and used with success in references [15] and [25]:

$$I(t) = I(0) \int_{\gamma=0}^{\infty} \Phi(\gamma) e^{-\gamma t} d\gamma \tag{2}$$

with a log-normal distribution function of the form:

$$\Phi(\gamma) = A \ \exp(-\frac{\ln^2(\gamma/\gamma^{MF})}{w^2}) \tag{3}$$

where γ^{MF} is the most-frequent decay rate corresponding to the maximum of $\Phi(\gamma)$, and w is a dimensionless width parameter. The decays are fitted on more than two decades (see fig.6) with only two free parameters γ^{MF} and w by a least squares fit with $1/y$ weighting of the data (y being the data value I(t)).

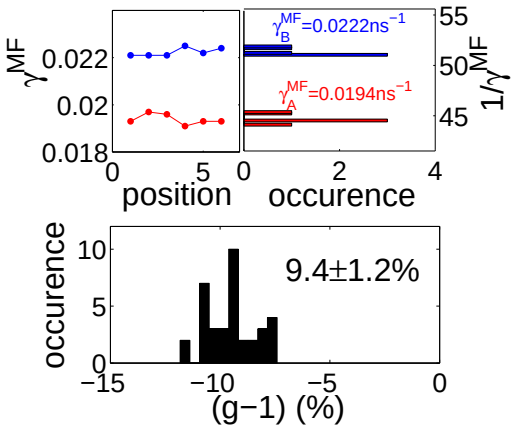

FIG. 7: (a) Most frequent decays γ^{MF} measured in the opals A (red line) and B (blue line) on six different positions. (b) Theoretical pseudogap-related pourcentage of difference between opals A and B (g-1) (see equation 7).

The figure7 presents the most frequent decays γ^{MF} measured in the opals A and B on six different positions.

The mean value of decay rates with their standard deviation are summaries in table I.

TABLE I: Mean most frequent decay rate $\langle\gamma^{MF}\rangle$ and width parameter $\langle w\rangle$ of the distribution for opals A and B, at 700nm detection wavelength with their standard deviations $\sigma(w)$ and $\sigma(\gamma)$. The percentage of decay rate variations of opal A with respect to opal B are given in the fourth column.

	opal A	opal B	difference
	$D_A = 269nm$	$D_B = 391nm$	
$\langle\gamma^{MF}\rangle$	$0.0222ns^{-1}$	$0.0192ns^{-1}$	-12.8%
$\sigma(\gamma^{MF})$	$0.0002ns^{-1}$	$0.0002ns^{-1}$	1.1%
$\langle w\rangle$	0.65	0.48	
$\sigma(w)$	0.03	0.05	
$\langle\gamma^{MF}\rangle/n^{eff}$	$0.0172ns^{-1}$	$0.0150ns^{-1}$	$-9.4\pm1.2\%$

We calculate the relative difference $(\gamma_A^{MF} - \gamma_B^{MF})/\gamma_B^{MF}$ by considering all possible pairs of positions on opals A and B and averaging over the corresponding 36 values. We obtain a fluorescence inhibition of 12.8% for the nanocrystals embedded in opal A with respect to

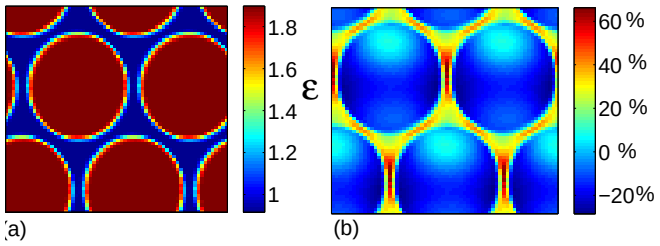

FIG. 8: (a) Assumed opal dielectric constant on a plane (111) for opal A. Calculation resolution: 36 nm for 391nm balls size opal. The transition zone between silica and air has a width of 108nm (b) Calculated percentage of variation of the local density of state around its mean value in the primitive cell in the pseudo gap for opal A at $a/\lambda = 0.79$ (for $a = \sqrt{2} \times 391nm$ and $\lambda = 700nm$).

the nanocrystals in opal B, with a standard deviation of 1.1%.

In order to explain this lifetime modification, the variation of the local density of states at the emitter positions has been calculated. According to Fermi's golden rule, the excited state of an emitting dipole decays exponentially to the ground state with a decay constant:

$$\gamma = \frac{2\pi}{\hbar^2} \sum_{n,\vec{k} \in BZ} | \vec{\mu} \, . \, \vec{E_{\vec{k}}} \, (\vec{r})|^2 \delta(\omega - \omega_{n,\vec{k}}) \tag{4}$$

where $\vec{\mu}$ is the dipole moment, and $\vec{E_{\vec{k}}} \, (r)$, a plane wave function, is the electric field of mode $\vec{k}$. n refers to the number of the band. The non radiative decay channels can be neglected [35]. The dipole moment $\vec{\mu}$ is assumed to be constant and randomly oriented in space. The decay rate when averaged over all orientations becomes:

$$\gamma = \frac{2\pi}{3\hbar^2} | \vec{\mu} |^2 \sum_{n,\vec{k} \in BZ} |E_{\vec{k}}(\vec{r})|^2 \delta(\omega - \omega_{n,\vec{k}}) = \frac{2\pi}{3\hbar^2} | \vec{\mu} |^2 \rho(\omega, \vec{r}) \tag{5}$$

$\rho(\omega, \vec{r})$ is the photon LDOS and is strongly dependent on the index modification at wavelength scale.

Starting from the band diagrams, the distribution of electromagnetic field is calculated in the first Brillouin zone by the standard plane-wave expansion method, and the LDOS inside the opal is inferred [12]. To improve the numerical accuracy, we used a linear interpolation technique as implemented within the abinit package [36] to obtain a stable numerical result with a small number of k points in the Brillouin zone: we used 7106 k points in the first Brillouin zone (equivalent to 79507 equally spaced k points). The primitive cell was

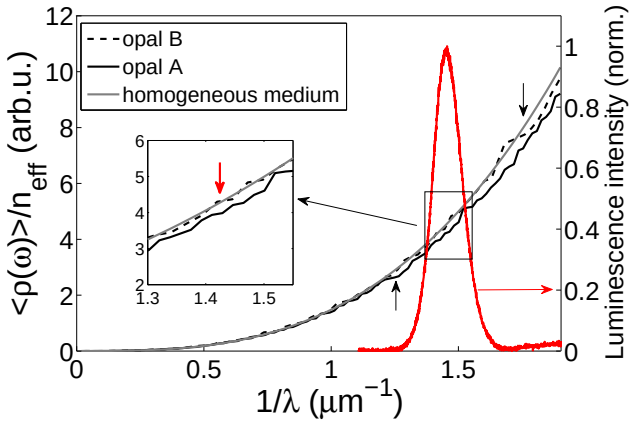

FIG. 9: Averaged ρ/n_{eff} ratio at air/SiO_2 interface for opal A (black line) and B (dash line), homogeneous medium (gray line). For the opals, the LDOS is averaged on regions for which the dielectric constant varies between 1.1 and 1.9 for opal A and between 1.1 and 2 for opal B. Green line: luminescence spectra of nanocrystals emitting at 685nm as a function of $1/\lambda$. The black arrows indicate the appearance of a pseudogap. The red arrow indicate the 700nm detection of our experiment.

divided into 32x32x32 segments, giving a resolution of 36nm considering 391nm balls size. For numerical reasons, the sharp transition between the silica and air dielectric constants lead to diverging results and had to be replaced by a smoother one, of thickness equal to 3x36=108nm (see fig. 8a).

The calculation of LDOS were performed with a silica index of 1.39 for opal A and 1.44 for opal B (values deduced from Bragg's fit in section II). As seen on figure 8b, the LDOS variation in opal A $\rho(\omega, \vec{r})$ over the cell is high and can become larger than 80% between voids and inner silica balls. As a consequence, in the simulations, the exact localization of the nanocrystals is critical, as their total diameter (core+ligands) is close to 10nm. We assume that nanocrystals are randomly located in the three pixels interface between air and silica, and we calculate the average LDOS (<LDOS>= $< \rho(\omega, \vec{r}) >$) for the opal A over this intermediate region for which the dielectric constant varies between 1.1 and 1.9 (between 1.1 and 2 for opal B).

Apart from bandgap effects, our experimental lifetime difference might be explained just by the small effective index difference between opals A ($n_A^{eff} = 1.29$) and B ($n_B^{eff} = 1.34$), as the decay rate in a homogeneous medium is proportional to the medium index. In order

to distinguish the index-difference effect ($n_A^{eff}/n_B^{eff} = 0.962$) from the pure bandgap effect, we write:

$$\frac{\gamma_A}{\gamma_B} = \frac{n_A^{eff}}{n_B^{eff}} \times g \tag{6}$$

where g is the pseudogap effect which is analysed in this paper:

$$g = \frac{\rho_A/n_A^{eff}}{\rho_B/n_B^{eff}} \tag{7}$$

On figure 9, we plot $\langle\rho(\omega)\rangle/n^{eff}$ as the function of the emission wave number $1/\lambda$, for opals A and B and for a homogeneous medium.

We can distinguished three different regimes on these curves.
For a wave number $1/\lambda < 1.21\mu m^{-1}$ we are below the gap of both opals and both LDOS can be described by the LDOS of a homogeneous medium (which scales as λ^{-3}). The small difference between the calculated LDOS and the λ^{-3} curve is attributed to noise of numerical origin and provides an estimate of the corresponding error (2%).

For $1/\lambda$ between 1.21 and $1.70\mu m^{-1}$, opal B still behaves like a homogeneous medium, but the LDOS of opal A is modified due to the presence of the photonic pseudogap. Like in the previous section, the opal B can be used as a reference in order to evidence the pseudogap effects in opal A in this spectral range.

When $1/\lambda$ is above $1.70\mu m^{-1}$, photonic effect are expected on both opals.

From the value of these curves at $\lambda = 700nm$, we calculate the theoretical pseudogap-related ratio between opal A and the homogeneous medium: g=0.93 (with the previously mentioned numerical error 0.02).

By averaging over all experimental 36 values of g, we find the experimental pseudogap-related decay difference between opals A and B : $g - 1 = 9.4\%$ (see figure 7 and table I) with a standard deviation of 1.2%. This result is in good agreement with the $g - 1 = 7 \pm 2\%$ theoretical value obtained from the above LDOS calculation, and within the experimental and numerical margins of error.

One might want to performed a comparison between nanocrystals in opal A and nanocrystals in opal A filled with decane, since it was taken as the reference in the previous section. Experimental pseudogap effect ratio g=0.98 was measured, in comparison with a theoretical value of 0.93. In this case, the difference between experimental and theoretical values

is slightly outside our margin of error and suggests that other effects could be included in lifetime modification calculations. Such conclusion was given in reference [12] to explain larger variations of lifetime compared with LDOS predictions for molecules embedded in colloidal photonic crystals. For single nanocrystals on glass coverslips, large decay rate fluctuations have been reported and attributed to the opening of non-radiative decay channels due to defects at the sample surface [37]. Other effects like local field electronic environment corrections may cause lifetime modification as considered in reference [38].

V. CONCLUSIONS

Opals prepared by sedimentation techniques and infiltrated by colloidal CdTeSe semiconductor nanocrystals have demonstrated a sufficient quality at a macroscopic scale to induce a modification of both the spectrum and lifetime of the nanocrystals emission. The dependence of the intensity with the collection angle is large and its dependence on detection wavelength has been described by Bragg's law. The emission lifetime was compared in an opal presenting a pseudogap effect at the emission wavelength and a reference opal for which emission is outside the gap. An experimental variation of 12.8% was measured and attributed to effective index difference between the opals (known to be 3.8% from reflection experiments) and the pseudogap effect (for which we deduce an experimental value of 9.4%). These results are close to the theoretical value of 7% obtained from numerical LDOS calculations.

A more significant influence of the photonic bandgap on the lifetime would require a larger index contrast, or an inverse opal for which complete photonic bandgap can be achieved. The insertion of a defect [39, 40] inside opals, inducing a large modification of the LDOS, is a promising alternative to monitor the lifetime of nanocrystals embedded in 3D photonic crystals.

Acknowledgments

Thomas Pons, Benoit Mahler and Benoit Dubertret are warmly acknowledged for the synthesis of the high quality CdTeSe nanocrystals which were crucial to the success of this study.

The authors also gratefully acknowledge Karel Kunc for helpfull discussions and Emmanuelle Lacaze for AFM measurements. This study was supported by the Russian Foundation for Basic Research (projects N 07-02-90000 and N 07-02-92176) and C'Nano Ile de France.

[1] S. Laurent, S. Varoutsis, L. Le Gratiet, A. Lemaitre, I. Sagnes, F. Raineri, A. Levenson, I. Robert-Philip, and I. Abram, Applied Physics Letters 87 (2005).

[2] O. Gauthier-Lafaye, D. Mulin, S. Bonnefont, X. Checoury, J. Lourtioz, A. Talneau, and F. Lozes-Dupuy, IEEE Photonics Technology Letters 17, 1587 (2005).

[3] G. Ruani, C. Ancora, F. Corticelli, C. Dionigi, and C. Rossi, Solar Energy Materials and Solar Cells 92, 537 (2008).

[4] T. D. Happ, I. I. Tartakovskii, V. D. Kulakovskii, J.-P. Reithmaier, M. Kamp, and A. Forchel, Phys. Rev. B 66, 041303 (2002).

[5] W.-H. Chang, W.-Y. Chen, H.-S. Chang, T.-P. Hsieh, J.-I. Chyi, and T.-M. Hsu, Physical Review Letters 96, 117401 (2006).

[6] K. Hennessy, A. Badolato, M. Winger, D. Gerace, M. Atatuere, S. Gulde, S. Faelt, E. L. Hu, and A. Imamoglu, Nature 445, 896 (2007).

[7] T. Yoshie, A. Scherer, J. Hendrickson, G. Khitrova, H. Gibbs, G. Rupper, C. Ell, O. Shchekin, and D. Deppe, Nature 432, 200 (2004).

[8] N. Ganesh, W. Zhang, P. C. Mathias, E. Chow, J. A. N. T. Soares, V. Malyarchuk, A. D. Smith, and B. T. Cunningham, Nature Nanotechnology 2, 515 (2007).

[9] V. Reboud, N. Kehagias, M. Zelsmann, M. Striccoli, M. Tamborra, M. Curri, A. Agostiano, D. Mecerreyes, J. Alduncin, and C. Sotomayor Torres, Microelectronic Engineering 84, 1574 (2007).

[10] S. G. Romanov, M. Bardosova, D. E. Whitehead, I. M. Povey, M. Pemble, and C. M. S. Torres, Applied Physics Letters 90, 133101 (2007).

[11] E. Yablonovitch, Phys. Rev. Lett. 58, 2059 (1987).

[12] Z.-Y. Li and Z.-Q. Zhang, Phys. Rev. B 63, 125106 (2001).

[13] V. Solovyev, Journal of Applied Physics 94, 1205 (2003).

[14] M. Megens, J. E. G. J. Wijnhoven, A. Lagendijk, and W. L. Vos, Phys. Rev. A 59, 4727 (1999).

[15] I. S. Nikolaev, P. Lodahl, A. F. van Driel, A. F. Koenderink, and W. L. Vos, Phys. Rev. B 75, 115302 (2007).

[16] P. Lodahl, A. F. van Driel, I. S. Nikolaev, A. Irman, O. Karin, D. Vanmaekelbergh, and W.

L. Vos, Letters to Nature 430, 654 (2004).

[17] M. Barth, R. Schuster, A. Gruber, and F. Cichos, Phys. Rev. Lett. 96, 243902 (2006).

[18] A. Blanco, C. Lopez, R. Mayoral, H. Miguez, F. Meseguer, A. Mifsud, and J. Herrero, Applied Physics Letters 73, 1781 (1998).

[19] Y. A. a. Valsov, Applied Physics Letters 71, 1616 (1997).

[20] Y. Lin, J. Zhang, E. H. Sargent, and E. Kumacheva, Applied Physics Letters 81, 3134 (2002).

[21] C. M. Chuang, W. B. Lu, W. F. Su, C. M. Lin, and Y. F. Chen, Journal of Applied Physics 97, 096104 (2005).

[22] K. Liu, T. Schmedake, K. Daneshvar, and R. Tsu, Microelectronics Journal 38, 700 (2007).

[23] S. Gaponenko, Journal of Luminescence 87-89, 152 (2000).

[24] S. G. Romanov, T. Maka, C. M. S. Torres, M. Müller, and R. Zentel, Journal of Applied Physics 91, 9426 (2002).

[25] R. A. L. Vallée, K. Baert, B. Kolaric, M. V. der Auweraer, and K. Clays, Phys. Rev. B 76, 045113 (2007).

[26] M. Barth, A. Gruber, and F. Cichos, Phys. Rev. B 72, 085129 (2005).

[27] M. Romanelli, C. Vion, C. Barthou, P. Benalloul, J. Frigerio, and A. Maitre, Journal of the Korean Physical Society 52, 1589 (2008).

[28] A. N. Gruzintsev, G. A. Emel'chenko, V. M. Masalov, M. Romanelli, C. Barthou, P. Benalloul, and A. Maitre, Inorganic Materials 44, 159 (2008).

[29] S. G. Johnson and J. D. Joannopoulos, Opt. Express 8, 173 (2001).

[30] Y. Xia, B. Gates, and S. Park, Journal of Lightwave Technology 17, 1956 (1999).

[31] I.A.Karpov, E.N.Samarov,V.M.Masalov,S.I.Bozhko, and G.A. Emel'chenko, Physics of the Solide State 47, 347-351 (2005)

[32] S. G. Romanov, T. Maka, C. M. Sotomayor Torres, M. Müller, R. Zentel, D. Cassagne, J. Manzanares-Martinez, and C. Jouanin, Phys. Rev. E 63, 056603 (2001).

[33] T.Pons et al, *Synthesis of Near Infrared Emitting Water Soluble CdTeSe/CdZnS Core/Shell Quantum Dots*, submitted

[34] A.F. van Driel, I.S. Nikolaev, P. Vergeer, P. Lodahl, D. Vanmaekelbergh, and W.L. Vos, Phys. Rev. B 75, 035329 (2007).

[35] X. Brokmann, L. Coolen,M. Dahan,and J.P. Hermier, Phys. Rev. Lett. 93, 107403-4 (2004)

[36] X. Gonze, J. M. Beuken, R. Caracas, F. Detraux, M. Fuchs, G. M. Rignanese, L. Sindic, M.

Verstraete, G. Zerah, F. Jollet, et al., Computational Materials Science 25, 478 (2002).

[37] G. Schlegel, J. Bohnenberger, I. Potapova and A. Mews, Phys. Rev. Lett. 88, 137401 (2002) ; B. R. Fisher, H.-J. Eisler, N. E. Stott and M. G. Bawendi, J. Phys. Chem. B 108, 143 (2004).

[38] S. F. Wuister, C. de Mello Donega and A. Meijerink, J. Chem. Phys. 121, 4310 (2004)

[39] P. Massée, S. Reculusa, K. Clays, and S. Ravaine, Chemical Physics Letters 422, 251 (2006).

[40] E. Palacios-Lidon, J. Galisteo-Lopez, B. Juarez, and C. Lopez, Advanced Materials 16, 341 (2004).

	opal A	opal B	difference
	$D_B = 269nm$	$D_A = 391nm$	
$\langle \gamma^{MF} \rangle$	$0.0222ns^{-1}$	$0.0192ns^{-1}$	-13.2%
$\sigma(\gamma^{MF})$	$0.0002ns^{-1}$	$0.0002ns^{-1}$	1.2%
$\langle w \rangle$	0.70	0.55	
$\sigma(w)$	0.03	0.04	
$\langle \gamma^{MF} \rangle / n^{eff}$	$0.0172ns^{-1}$	$0.0143ns^{-1}$	$-9.9 \pm 1.2\%$

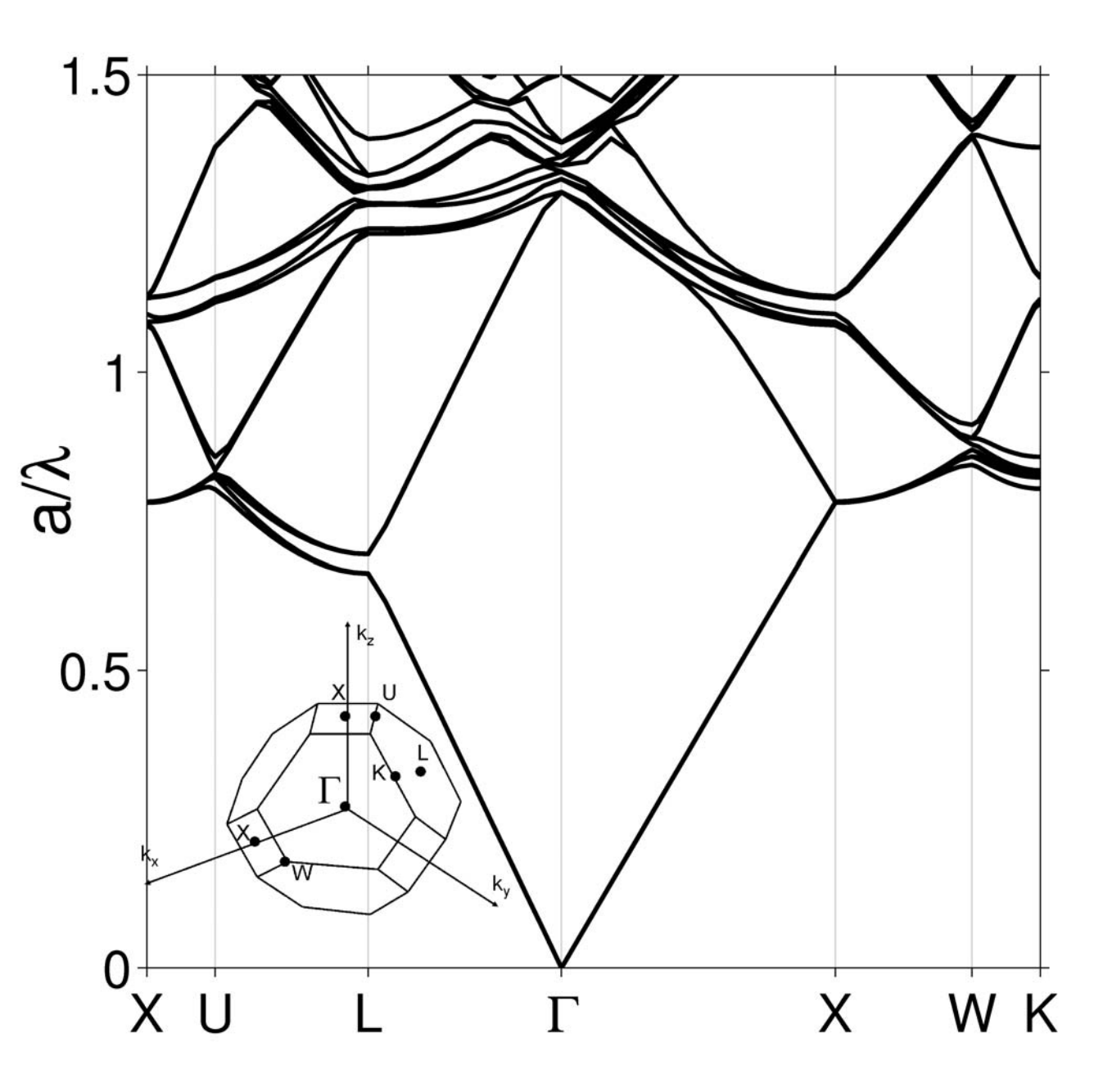
1.5
1
0.5
0
a/λ
X
U
L
Γ
X
W
K
k_z
X
U
L
K
Γ
X
W
k_x
k_y

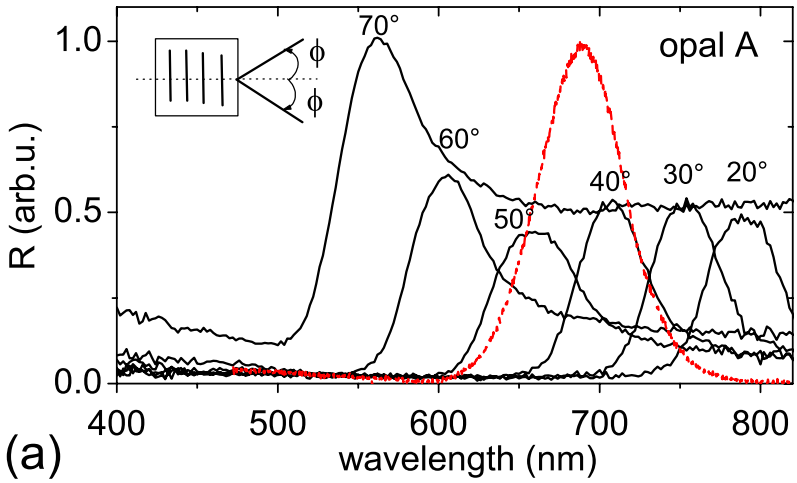
opal A
70°
60°
50°
40°
30°
20°
ϕ
ϕ
R (arb.u.)
wavelength (nm)
1.0
0.5
0.0
400
500
600
700
800

(a)

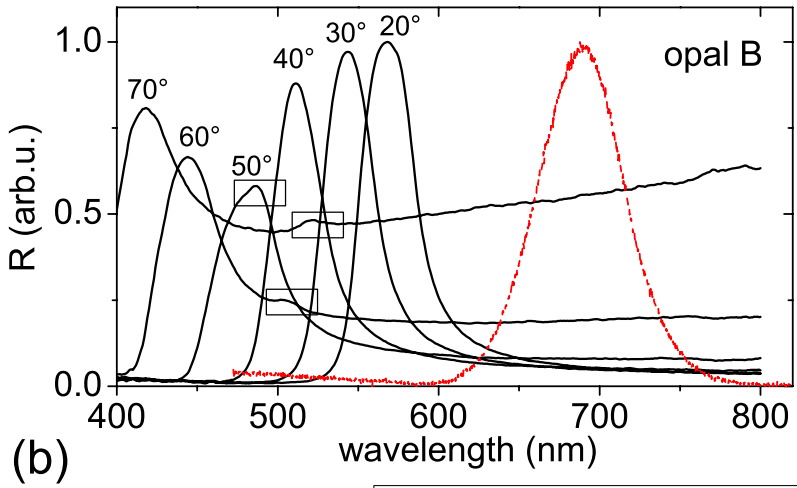
opal B
70°
60°
50°
40°
30°
20°
R (arb.u.)
wavelength (nm)
1.0
0.5
0.0
400
500
600
700
800

(b)

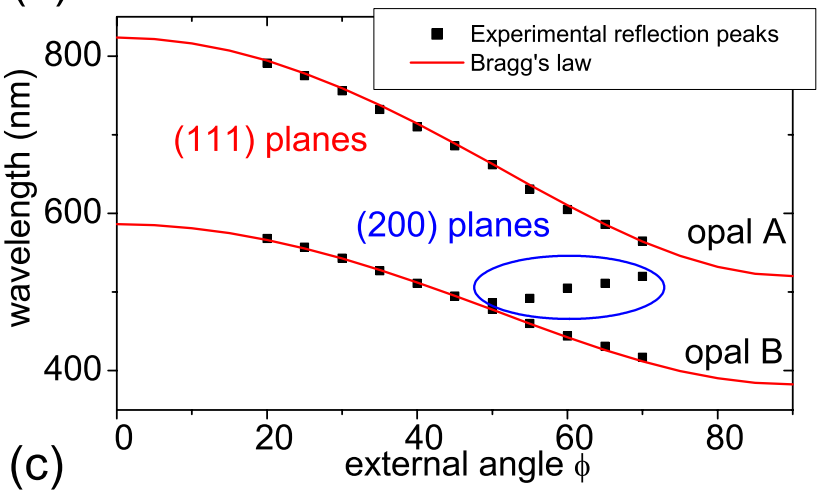
Experimental reflection peaks
Bragg's law
(111) planes
(200) planes
opal A
opal B
wavelength (nm)
external angle ϕ
800
600
400
0
20
40
60
80

(c)

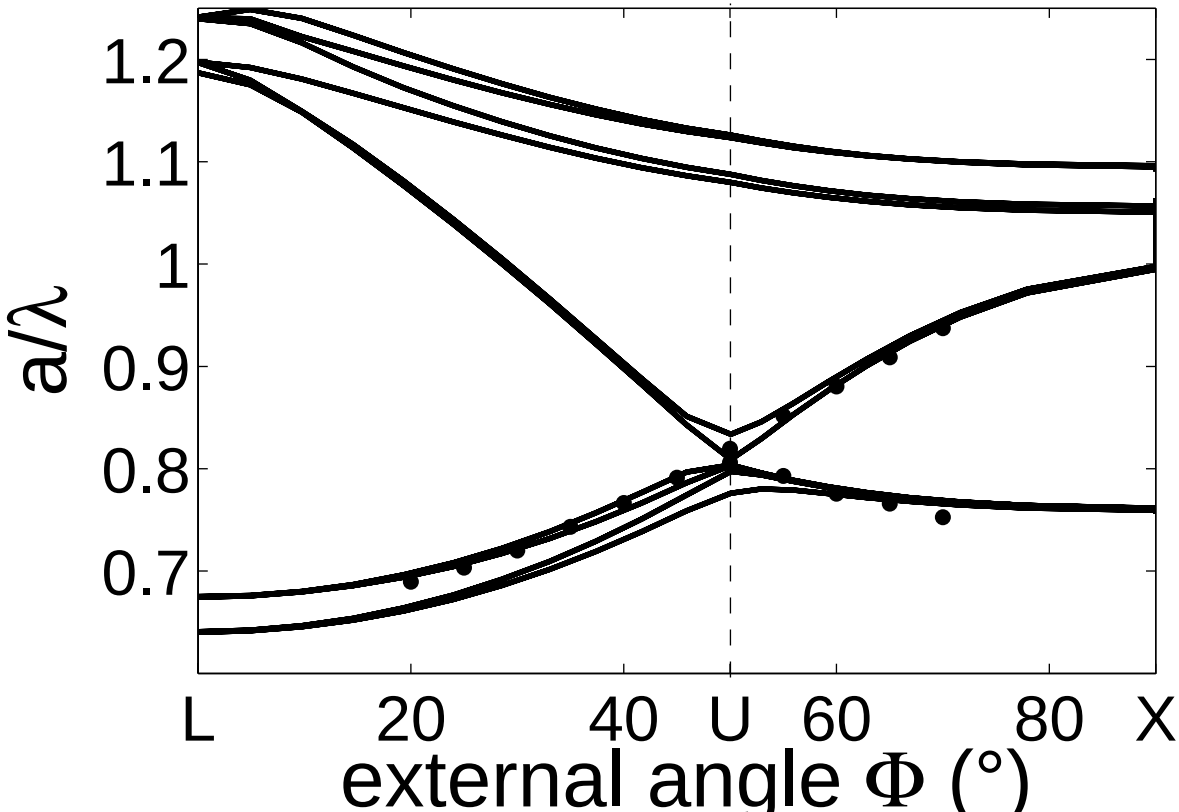
1.2
1.1
1
0.9
0.8
0.7
a/λ
L
20
40
U
60
80
X
external angle Φ (°)

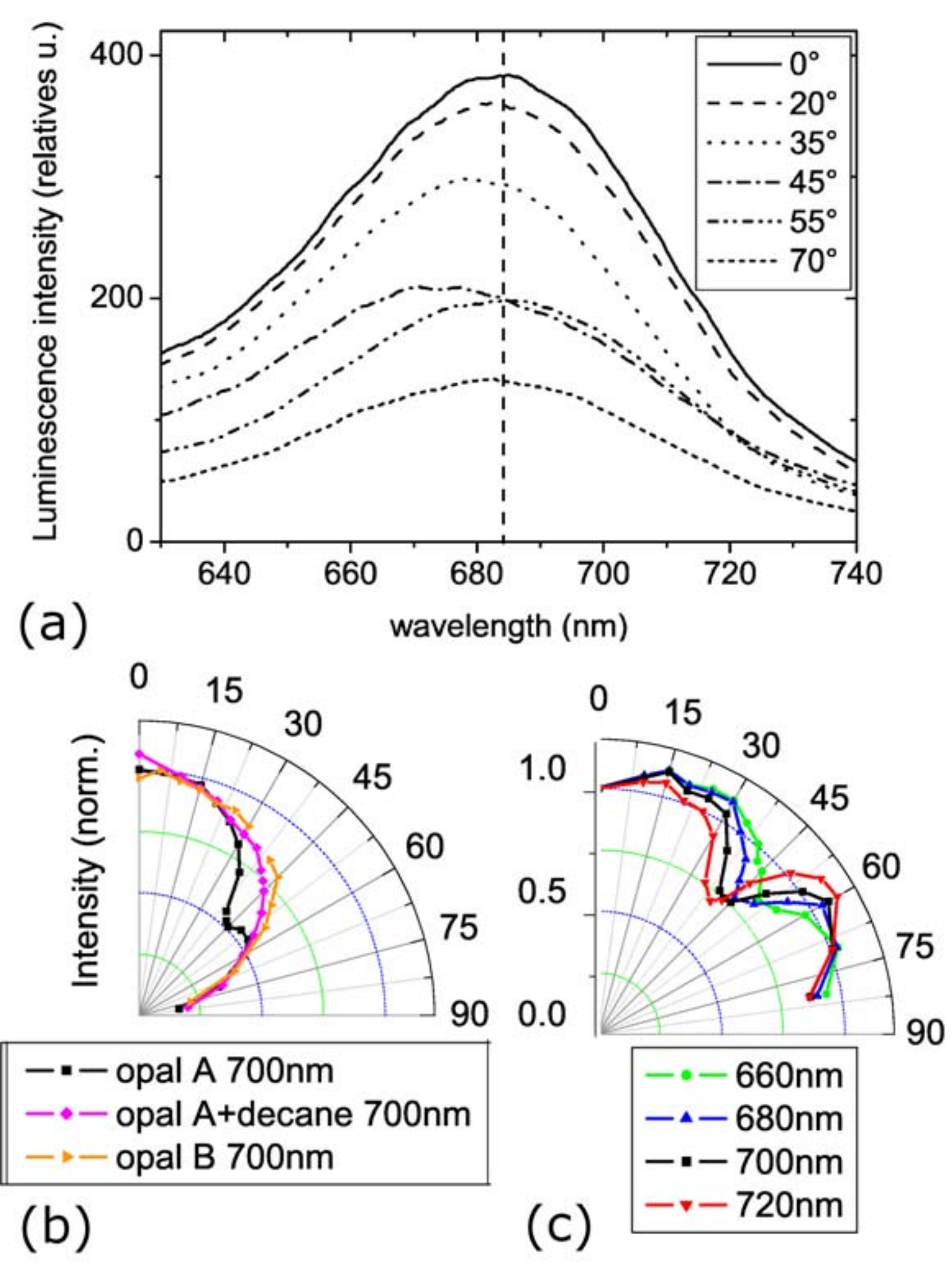
Luminescence intensity (relatives u.)
400
200
0
640
660
680
700
720
740
wavelength (nm)
0°
20°
35°
45°
55°
70°
(a)
0
15
30
45
60
75
90
Intensity (norm.)
opal A 700nm
opal A+decane 700nm
opal B 700nm
(b)
1.0
0.5
0.0
660nm
680nm
700nm
720nm
(c)

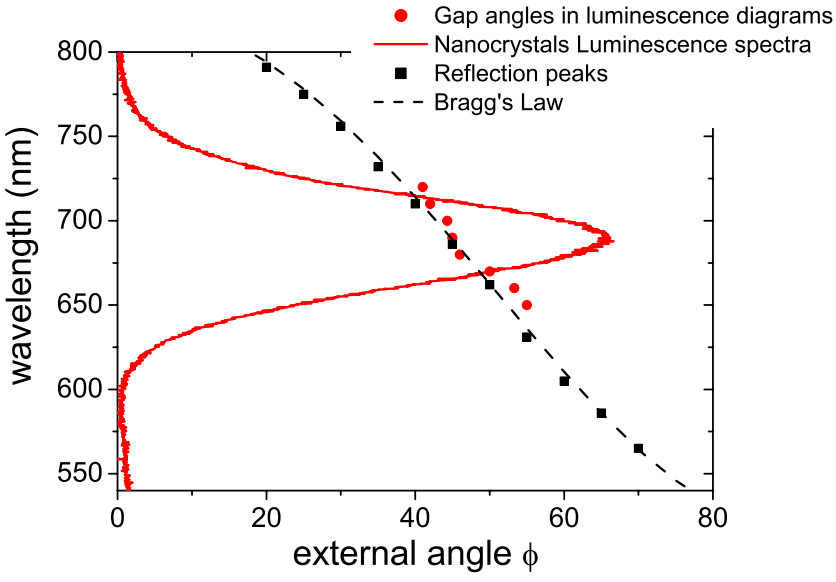
Gap angles in luminescence diagrams
Nanocrystals Luminescence spectra
Reflection peaks
Bragg's Law
wavelength (nm)
800
750
700
650
600
550
0
20
40
60
80
external angle ϕ

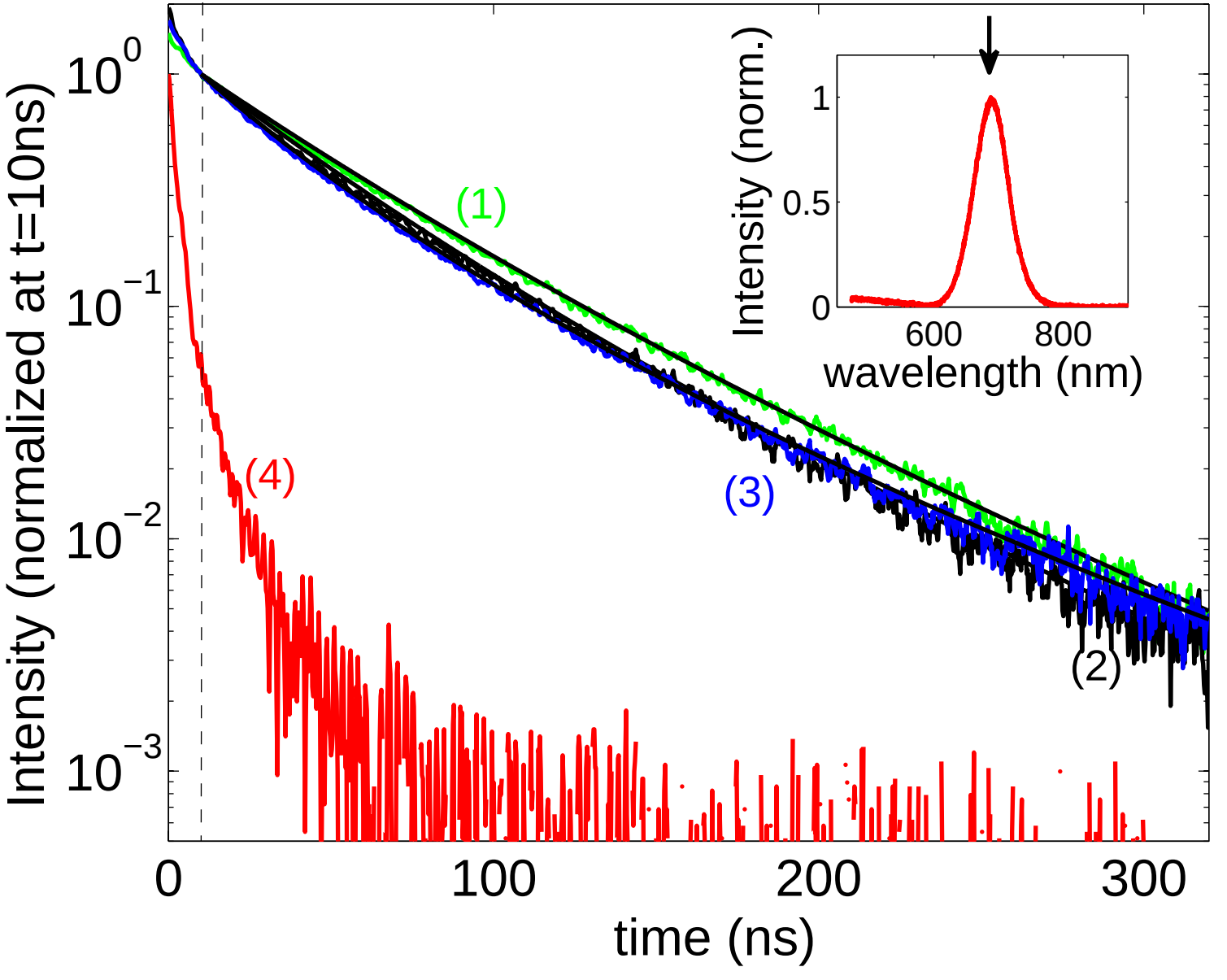
Intensity (normalized at t=10ns)
10^{0}
10^{-1}
10^{-2}
10^{-3}
0
100
200
300
time (ns)
(1)
(2)
(3)
(4)
Intensity (norm.)
1
0.5
0
600
800
wavelength (nm)

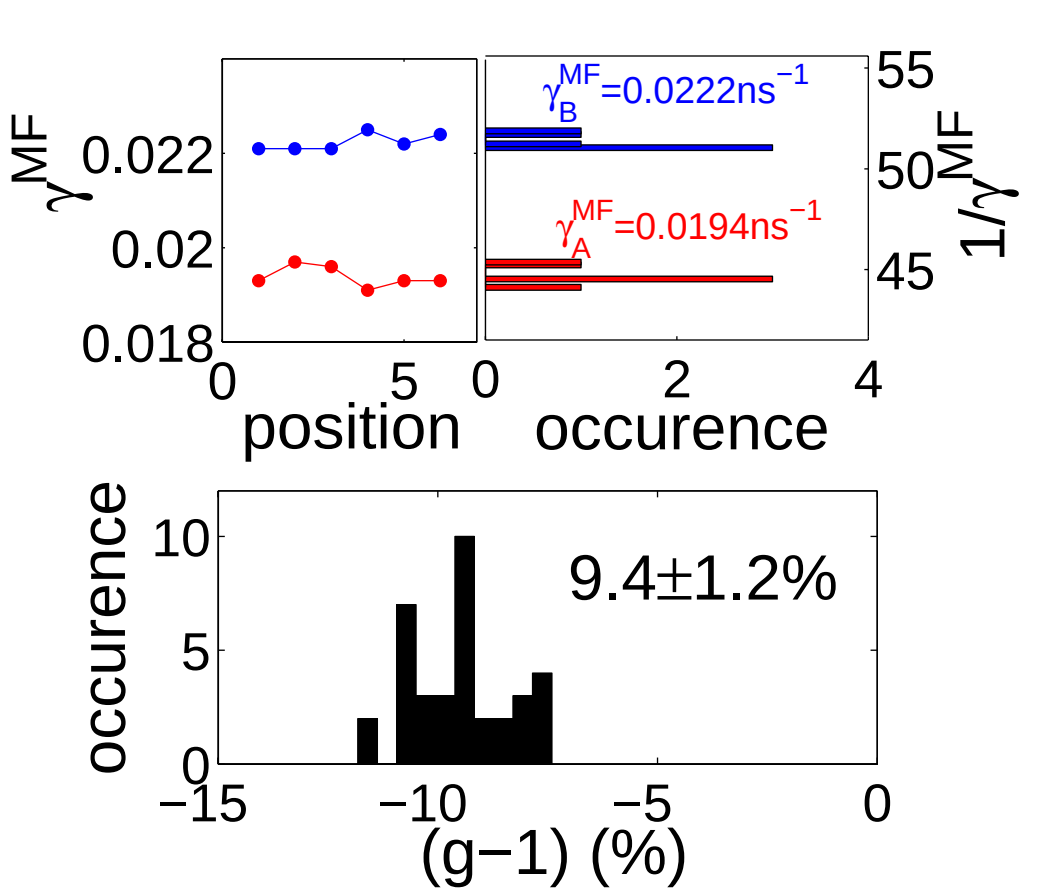
γ^{MF}
0.022
0.02
0.018
0
5
position
γ_B^{MF}=0.0222ns^{-1}
γ_A^{MF}=0.0194ns^{-1}
55
50
45
$1/\gamma^{MF}$
0
2
4
occurence
occurence
10
5
0
9.4±1.2%
−15
−10
−5
0
(g−1) (%)

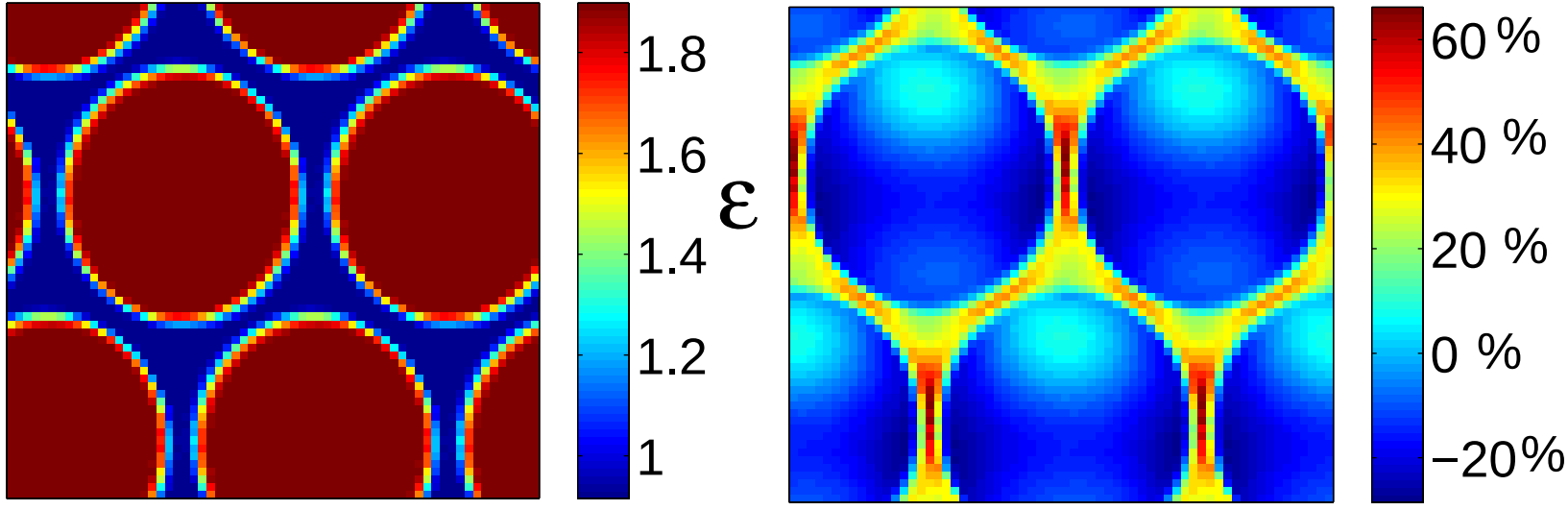
1.8
1.6
1.4
1.2
1
ε
60 %
40 %
20 %
0 %
−20%
(a)
(b)

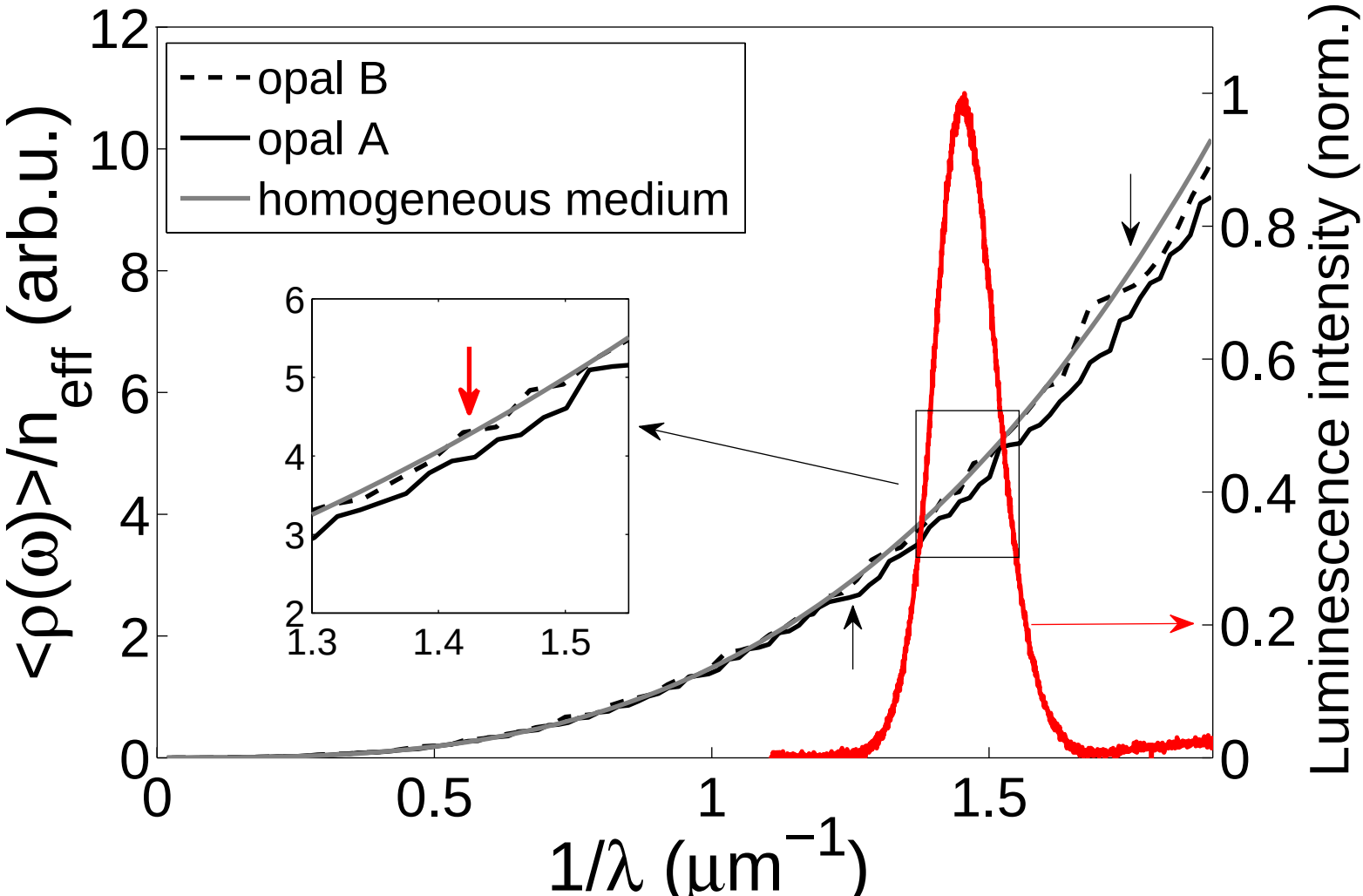
opal B
opal A
homogeneous medium
<ρ(ω)>/n_eff (arb.u.)
Luminescence intensity (norm.)
1/λ (μm^−1)
0
2
4
6
8
10
12
0.2
0.4
0.6
0.8
1
0.5
1.5
3
5
1.3
1.4